Semi-Annual Report Submitted to the
National Aeronautics and Space Administration

For January - June, 1999

Contract Number: NAS5-31370

Land Surface Temperature Measurements from EOS MODIS Data

MODIS Team Member
PRINCIPAL INVESTIGATOR

ZHENGMING WAN

P.I.'s Address:

Institute for Computational Earth System Science
University of California
Santa Barbara, CA 93106-3060

phone : (805) 893-4541
Fax no: (805) 893-2578
Internet: wan@icess.ucsb.edu

Land Surface Temperature Measurements from EOS MODIS Data

Semi-Annual Report for January - June, 1999

Zhengming Wan

Abstract

A recent revision of the MODIS Land-Surface Temperature Algorithm Theoretical Basis Document (LST ATBD) was completed in April. A paper on the vicarious calibration of MODIS Airborne Simulator (MAS) thermal infrared channels based on the MAS data and field measurement data acquired in the field campaign conducted in Mono Lake, California, on March 10, 1998, was submitted in February, revised in June and accepted in July. The at-launch version of the MODIS Proto-Flight Model (PFM) relative spectral response (RSR) function was used to generate the look-up tables that will be used in the operational generation of the at-launch MODIS LST products. Comprehensive tests of the MODIS LST code were made jointly with the MODIS Science Data Support Team (SDST) using the simulated MODIS data. Measurements of the atmospheric temperature and water vapor profiles were made in a field campaign conducted in the Mono Lake area in late March and early April in order to obtain some information of the annual variation in the clear-sky atmospheric conditions during the winter/spring reasons over the area. A PC video card is used to store temperature images from an AGEMA IR camera on disk at a higher speed. It was confirmed that the error in the temperature images can be significantly reduced by temporal and spatial averages. This makes it possible for the IR camera to provide useful information of the LST temporal and spatial variations in the field campaigns that have been planned for the vicarious calibration of MODIS TIR channels and the validation of MODIS LST products. Numerical simulations have been initiated for the development of LST algorithms for the MODIS PM model.

Recent Paper Accepted

Z. Wan, Y. Zhang, X. Ma, M. D. King, J. S. Myers, and X. Li, "Vicarious calibration of MODIS Airborne Simulator (MAS) thermal infrared channels", Applied Optics, original manuscript submitted in February, revised in June, and accepted in July 1999.

1. Revision of the MODIS LST ATBD and a MAS Vicarious Calibration Paper

A recent revision of the MODIS Land-Surface Temperature Algorithm Theoretical Basis Document (LST ATBD) was completed in April (access to http://modarch.gsfc.nasa.gov/MODIS/ATBD/atbd.html for atbd_mod11.pdf, v3.3, 4/30/99). The updates in this version include new results of the calibration and validation activities, the classification-based emissivity look-up table (Snyder et al, 1998) used in the generalized split-window LST algorithm, and the basic atmospheric profiles selected for the establishment of the look-up tables that will be used in the day/night LST algorithm in the at-launch LST code.

A paper on the vicarious calibration of MAS thermal infrared (TIR) channels based on the MAS data and field measurement data acquired in the field campaign conducted in Mono Lake, California, on March 10, 1998, was submitted in February, revised in June, and accepted in July 1999. Results in the paper were given in the semi-annual report for July - December, 1998, for Contract Number NAS5-31370. The significance of this study is shown not only by giving results comparable with those from previous studies based on comparisons with High Resolution Interferometer Sounder (HIS) data and giving results for more TIR channels but also by demonstrating the advantages of using high elevation sites under dry atmospheric conditions as vicarious calibration sites. For such calibration sites, well calibrated high spectral resolution airborne instruments are not necessary as long as ground-based instruments can provide accurate spectral surface-leaving radiance or accurate surface temperature and spectral surface emissivity, and atmospheric temperature and water vapor profiles at reasonable accuracies. Without requiring a flight of a well calibrated high spectral resolution airborne instrument for each ground-based vicarious calibration activity, it will be easy to schedule the calibration field campaigns and to conduct a field campaign at a lower cost. Hence it will be possible to conduct more small-scale vicarious calibration field campaigns at different sites in order to evaluate the calibration accuracy of the MODIS TIR channels over a wide range of scene temperatures.

2. Updates of the Look-up Tables Used in the At-launch LST Code

The at-launch version of the MODIS Proto-Flight Model (PFM) relative spectral response (RSR) function, which was released in May, was used to update the following look-up tables (LUT): LUT3 for the coefficients of the generalized split-window LST algorithm, LUT4 for the conversion of band radiance to band brightness temperature, LUT5 for the atmospheric and solar radiation terms used in the day/night LST algorithm, and LUT6 for the regression coefficients of the day/night LST algorithm. Note that LUT3-6 are referred to the look-up tables mentioned in the v3.3 LST ATBD. These LUTs will be used in the operational product generation of the at-launch MODIS LST products.

It is most difficult to build the last two LUTs. The establishment of LUT5 takes three major steps. In step 1, we carefully select basic atmospheric profiles so that they can accommodate the wide range of atmospheric variations through shifting the temperature profile (T shifting) and scaling the water vapor

profile (wv scaling) as described in section 3.1.2.3 of the LST ATBD. In step 2, we make accurate radiative transfer simulations for all the cases of the selected basic atmospheric profiles and their variants. In step 3, we calculate the band averaged atmospheric and solar radiation terms with the spectral response function of the MODIS instrument as the weight. In the first step, we start with the four standard atmospheric profiles in the MODTRAN code (Berk et al., 1987) for mid-latitude summer and winter, sub-arctic summer and winter. We get eight basic atmospheric profiles by change the shape of the water vapor profile of these four standard profiles keeping their values of column water vapor unchanged. We also add one tropical atmospheric profile with surface temperature at 309.6 K and one cold atmospheric profile with surface temperature at 231.25 K. Then we search the best fitting with the ten basic atmospheric profiles through T shifting and wv scaling for each of 1532 clear-sky cases in the satellite TOVS Initial Guess Retrieval (SATIGR) atmospheric profile database (Moine et al., 1987) and calculate std δT and std δwv, the root mean-square difference of the temperature and water vapor values at elevation levels of 0, 1, 2, and 4km between the target profile and the basic profile after T shifting and wv scaling. We only try to fit the lower portion of the atmospheric profile at these four levels for computational efficiency because this portion of the atmosphere has the most strong effect on the atmospheric and solar radiation terms in the seven TIR channels used in the day/night LST algorithm. By adding the worst case of profile into the basic atmospheric profile database we can reduce the mean and maximum std δT and std δwv values. Repeat the above process until the maximum std δT and std δwv are acceptable. Finally we added two, one, and two more atmospheric profiles in the high, middle, and low temperature ranges, respectively. In the 15 basic atmospheric profiles, seven atmospheric profiles are in the low temperature range (air surface temperature $T_{sfc} \leq 274.35\,^{\circ}$K). Four of the seven profiles include temperature inversion layers at different strengths. If we define the inversion strength with the difference between air temperatures at the surface and at the elevation level 1km above the surface, there are two -1.9 °K, one -15.21 °K, and one -20.8 °K. Figure 1 shows the air surface temperature and column water vapor of the 15 basic atmospheric profiles, SATIGR profiles, and MAS profiles, i.e., the 52 atmospheric profiles used in the algorithm development of atmospheric temperature and water vapor retrieval from MAS data (A), and the errors in their profile fitting with the 15 basic atmospheric profiles (B). Note that the unit of water vapor density used in this figure is cm/km, which is equivalent to gram/(km*cm^2). In order to take land-surface elevation into considerations, we introduce additional 15 basic atmospheric profiles by lifting the lower portion (0-9km) of the temperature and water vapor profiles of the first set of 15 basic profiles for 4km. Figure 2 shows the histograms of the errors in temperature and water vapor profile fittings of the 1532 SATIGR profiles with the 15 basic atmospheric profiles. As shown in Fig. 2(A), 66% of SATIGR profiles fall in the std δT range of 0-3 K, 94% in the 0-5 K range, and 99% in the 0-6 K range. As shown in Fig. 2(B), 92% of the SATIGR profiles fall in the std δwv range of 0-0.1 cm/km.

After steps 2 and 3, we obtain two sets of the atmospheric and solar radiation terms for the 15 basic atmospheric profiles. The first set is for the atmospheric profiles which surface is at 0km and the second

set is for the atmospheric profiles which surface is at 4km above sea level. In real processing, the surface elevation of the 5km grid will be used to obtain the atmospheric and solar radiation terms required for the given surface elevation through interpolation or extrapolation. After testing the algorithm with real MAS and MODIS data over cold ranges, we may find that it is not necessary to keep all the four temperature-inversion profiles in the database of 15 basic atmospheric profiles because it may be difficult to retrieve the temperature inversion layers with the MAS and MODIS sounding channels.

3. Tests of the MODIS LST Code

The execution of the at-launch MODIS LST code (PGE16) is managed by its production rules and process control file (PCF) to process the input granules given in PCFs. The PGE16 will process approximately 240 1km-resolution granules, that cover land tiles, by the end of each day when all required input granule files become available. For each such input granule, PGE16 generates a final MOD11_L2 product file and generates/updates interim L3 LST product files (MOD11A1 and MOD11B1) for the tiles that intersect with the granule. After processing all daily granules, the interim 1km MOD11A1 and 5km MOD11B1 LST files become complete LST L3 products and then are ready for archive. A workstation based on a 500MHz Alpha 21264 CPU takes 5-10 minutes to complete a pair of day and night input granules (each contains five minutes of observations in about 2030 scan lines) depending on the percent of clear-sky land pixels in the input granules. The sizes of L2, 1km and 5km L3 LST files are 26MB, 23MB, and 1.2MB, respectively.

Comprehensive tests of the MODIS LST code were made jointly with the MODIS Science Data Support Team (SDST) using the simulated MODIS data at the Science Computing Facility (SCF) at the University of California, Santa Barbara, and the Team Leader Computing Facility (TLCF) at the NASA/Goddard Space Flight Center (GSFC). Prompt feedbacks were provided to the SDST in most of the time. Frequent discussions and e-mail exchanges were made on the results of the tests and on the details in appropriate implementation of the PGE16 production rules at the MODIS Data Processing System (MODAPS) at GSFC.

Parallel processing is allowed for the LST process through a zoning approach so that several CPUs can work on different zones of granules at the same time and only a single CPU can work on each tile any time during the PGE execution. In the recent X-day test on the SGI Origin 2000-based MODAPS, three CPUs were used to process the granules which centers fall in latitude zones of 60-90N, 0-30N, and 30-60S, respectively, in the first round. After all the processing on these three zones was completed, three CPUs were used to process the granules which centers fall in latitude zones of 30-60N, 0-30S, and 60-90S, respectively. The whole daily PGE16 execution took approximately seven hours. The results of the test were analyzed at the MODIS LST SCF and the Land Data Operational Product Evaluation (LDOPE) Facility. It was found that the main source of the problems is that some of the production rules had not been followed.

4. Progress on the Activities Related to the MODIS LST Validation

It was originally planned to conduct a calibration/validation field campaign over the area of Mono Lake, CA, in March 1999. ER-2 MAS flights were requested for this field campaign. The MAS flights were postponed due to the launch delay of the Earth Observing System (EOS) AM/Terra platform which was originally scheduled to launch in 1998. Correspondingly, we changed the field campaign plan. In late March and early April we only measured the atmospheric temperature and water vapor profiles in the Mono Lake area in order to obtain some information of the annual variation in the clear-sky atmospheric conditions during winter/spring reasons over the area. Figure 3 shows the atmospheric temperature and water vapor profiles measured near Mono Lake on March 10, 1998, and April 2, 1999. The atmospheric conditions on these two dates were both dry (column water vapor less than 0.4cm). This indicates that the dry atmospheric condition in winter/spring reasons over the Mono Lake area is sustainable so that it is suitable for the vicarious calibration of the TIR channels of airborne and satellite sensors as long as field measurements and MAS flights are made in really clear-sky days and in constant wind conditions.

One lesson learned from our field campaigns since 1995 is that we do not have enough data to determine the range of uncertainties in the comparisons between the LST measured by field instruments and the LST retrieved from airborne and/or satellite data due to the spatial variation in LST. The field-of-view (FOV) of ground-based TIR instruments ranges from 10cm to 50cm, while the MAS pixel size is 50m and the pixel size of MODIS TIR channels is 1km or larger. Therefore, it is critical to know the spatial variation in LST at the scales from several centimeters to at least 50m, at an accuracy good enough for the calibration/validation purpose. We purchased an IR camera (THERMOVISION 570) from AGEMA Infrared Systems in late 1997 and received the recalibrated IR camera in 1998. The detector used in this IR camera is a focal plane array of uncooled microbolometer with 320 x 240 elements in the spectral range of 7.5-13μm. The FOV of the camera is 24° by 18°. There are four options of temperature ranges available for user selection. Normally, the -20 to 120C range is suitable for our applications. The accuracy specification is ±2°C. In its standard mode, the image data can be stored on a PCMCIA hard disk card at a highest rate of one frame per second or lower rates. We checked the accuracy by placing the camera in front of a blackbody at temperature 25°C and storing 100 image frames. It was found that the accuracy of a single image is not good enough for our calibration/validation purpose. It is necessary to make an average image from approximately 100 images. This IR camera takes 5-7 minutes to store 100 images of the target scene plus 2-3 sets of 100 frames of blackbodies at 2-3 different temperatures for its accurate calibration. Such a speed is too low for our calibration/validation purpose. This IR camera can be upgraded to a high speed model (57 frames per second) with a special interface and specialized PC at approximately 60% of the original price of the IR camera. We did not take this approach because we prefer to upgrade the IR camera into a lightweight system with common components priced for the large commercial market in order to take the advantage of rapid advances in the personal computer industry. One option is to use a PC video card to grab temperature images from the AGEMA IR camera at a higher

speed. Currently a frame grabber card from Imaging Technology Incorporated is installed on a PC based on Intel Pentium II 300 MHz processor and Ultra ATA hard disk drive. Although this video card can grab the video signals from the AGEMA IR camera and to display the temperature image on the monitor screen at a rate of 30 frames per second, only 10 images can be stored every second on the hard disk of the PC with a code that we recently developed. This speed is 10 times the speed of storing images with a PCMCIA hard disk card. It is expected that the speed can be increased further by improving the code and by using a new PC based on Intel Pentium III CPU and high speed Ultra2 SCSI disk drive.

We tested the AGEMA IR camera in front of a blackbody at temperatures 10, 25, and 40 °C and stored three sets of 256 images on the disk space through the frame grabber card. The dimension of the stored temperature images is 640 x 480 pixels. By averaging every two lines and two pixels, the temperature images were converted into the format of 320 x 240 pixels, the original resolution of the detector in the IR camera. In order to analyze the effect of temporal average on the accuracy improvement we separate the 256 images into 16 groups, each containing 16 images. Each group of the 16 images were averaged into an averaged temperature image. Then we calculated the standard deviations, maximum and minimum temperature values of the original 256 images and the 16 averaged images for each blackbody temperature. Table I shows the errors in the AGEMA-measured temperature images of a blackbody at temperatures 10, 25, and 40 °C. A segment of the temperature image with a size of 120 x 120 pixels was selected in the middle portion of the blackbody image in order to avoid the possible effect of the temperature gradient of the blackbody by the edge on the error analysis of the IR camera. Part A is for the results from the original 256 image frame segments before the temporal averaging. Part B is for the results from the 16 averaged image frame segments. The mean temperature in the segment is -0.36, -0.29, and -0.34 °C off the blackbody temperatures in cases of 40, 25, and 10 °C. This indicates that both the IR camera and the blackbody are in good conditions of calibration. In order to secure the calibration accuracy, we need to calibrate the IR camera with a well calibrated blackbody before, during, and after field measurements. Although the segmental mean values of the standard deviation of the temperature error (std δT) is small (0.11 °C even in case of 10 °C) and the maximum std δT is smaller than 0.5 °C, the maximum error may as large as ±1.0 °C in case of 40 °C, and even worse in cases of low temperatures. By making average of 16 frames, the mean std δT is reduced by 30-40%, but the values of maximum std δT, maximum error are reduced only by 10-30% (by comparing Part B with Part A in the last three columns). This means that the high-frequency noise in each individual microbolometer element does not follow the Gaussian distribution. Figure 4 shows the maximum and minimum temperature values of the blackbody at 40 °C for each pixel in the segment of the temperature images measured by the AGEMA IR camera before (A) and after (B) the temporal averaging. Note that the temperature values have been calibrated with the blackbody temperature for the mean temperature in the segment. The pixel number was signed to every pixels in the first line of the segment and then to the next line until the last line in the segment. In Figure 4(A), more than 99% of the pixels fall in the temperature range of 40 ± 0.5 °C. In Figure 4(B), more than 99% of the

pixels fall in the temperature range of $40 \pm 0.3\,^{\circ}C$. But there are small numbers of pixels in large errors in both cases. As shown in Parts C-F of Table I, the errors are significantly reduced by the spatial average. In Parts C and D, every 2 x 2 pixels are averaged into a larger pixel. If the scene temperature is $40\,^{\circ}C$ or above, averaging by 2 x 2 pixels and by 16 frames (in Part D) is enough to make the error smaller than $0.32\,^{\circ}C$ in the worst case. In Parts E and F, every 4 x 4 pixels are averaged into a larger pixel. A combination of the spatial average by 4 x 4 pixels and the temporal average by 16 frames makes the error smaller than $0.32\,^{\circ}C$ for all the large pixels even in case of blackbody temperature at $10\,^{\circ}C$. The above analysis confirmed that the error in the temperature images measured by the AGEMA IR camera can be significantly reduced by temporal and spatial averages. As shown in Figure 5, the error in measured temperatures after the spatial average by 4 x 4 pixels and the temporal average by 100 frames is smaller than $0.2\,^{\circ}C$ and $0.25\,^{\circ}C$ at temperatures $40\,^{\circ}C$ and $10\,^{\circ}C$, respectively. Figure 5(A) reveals that there may be a temperature gradient of approximately $0.1\,^{\circ}C$ in the segment of the blackbody. An absolute accuracy of $0.25\,^{\circ}C$ is the goal for the field measurements of surface temperature in our vicarious calibration field campaigns. It should be pointed out that the spatial averaging of temperature values used in the above analysis is only valid for flat homogeneous scenes where the spatial variation in surface emissivities is negligible and the surface temperature varies only by a few degrees. Otherwise, we have to convert the temperature values into radiance values, to make spatial average of the radiance values, and then to convert the averaged radiance values back to averaged temperature values. This will be very difficult, if not impossible, to obtain accurate averaged temperature values through radiance averaging because of the uncertainties in the surface spectral emissivity and spectral response function of the IR camera. We can avoid this complicated procedure by conducting calibration/validation field campaigns only over flat homogeneous sites such as playa, lakes, and short-grass lands. The above results show that with the video card to grab temperature images from the IR camera and to store them on disk at a speed higher than 10 frames per second, the IR camera will be able to provide useful information of the LST temporal and spatial variations in the field campaigns that have been planned for the vicarious calibration of MODIS TIR channels and the validation of MODIS LST products.

Field campaigns planned for 1999 and 2000 are shown in Table II. A field campaign over Railroad Valley, NV, and the area of Mono Lake, CA, is scheduled for the period of September 20 to October 15, 1999. During this period, 16 ER-2 flight hours will be used for daytime and nighttime MAS flight missions. Airborne Visible-Infrared Imaging Spectrometer (AVIRIS) has been requested for daytime flight missions. The ER-2 flight schedule will be coordinated with Dr. Kurt Thome of the University of Arizona, who has also requested for an alternative platform for a MASTER (the MODIS and ASTER Airborne Simulator) flight to coincide with an overpass of Landsat-7 during this period of time. A vicarious calibration field campaign over the area of Mono Lake, CA, is planned for February/March 2000. MAS/AVIRIS flights have been requested for this campaign. A vicarious field campaign over Uyuni Salt Flats, Bolivia, is being planned for May 2000. There will be no MAS flight for this field campaign. A field campaign over

Railroad Valley, NV, and the area of Mono Lake, CA, is scheduled for June/July 2000 for the MODIS LST validation. MAS/AVIRIS flights have been requested for this campaign. Collaboration will occur during the ASTER's calibration/validation field campaign over Mauna Loa, Hawaii, in April-June 2000. MASTER flights have been requested during the PACRIM-II deployment. We will join the field campaign of SAFARI 2000 and to conduct ground-based TIR measurements over Makgadikgadi Salt Pans, Botswana, in August 2000. Close collaboration with the ASTER team and other groups will be kept for future MODIS LST validation activities, and new opportunities for collaboration in the international efforts to validate LST at the global scale will be pursued.

5. The Development of LST Algorithms for the MODIS PM Model

The refinement and development of the MODIS LST algorithm for the MODIS PM model was planned. The LST product PM-1 MOD11comb will contain Levels 2 and 3 land surface emissivity and temperatures retrieved through the combination of PM and AM/Terra MODIS data so that the retrieved surface temperature with a better diurnal feature will be more suitable for various applications. In the early post-launch period the PM-1 MOD11adv product will include Levels 2 and 3 land surface emissivity and temperatures retrieved by an advanced LST algorithm that also corrects the effects of thin cirrus clouds and aerosols with inputs from MODIS atmospheric products.

Numerical simulations have been initiated for the development of LST algorithms for the MODIS PM model. A close collaboration with Paul Menzel's atmospheric profile retrieval group at The University of Wisconsin-Madison was established in the development of new LST algorithms. Our research has been focused on the simultaneous retrieval of surface temperature and emissivity, and atmospheric temperature and water vapor profiles from simulated MAS data over wide ranges. Preliminary results are very promising. A paper on this research has been drafted and will be submitted to a scientific journal soon.

REFERENCES

Berk, A., L. S. Bemstein, and D. C. Robertson, ''MODTRAN: A moderate resolution model for LOWTRAN,'' Rep. AFGL-TR-87-0220, Burlington, MA: Spectral Sciences, Inc., 1987.

Moine, P., A. Chedin, and N. A. Scott, ''Automatic classification of air mass type from satellite vertical sounding data. Application to NOAA-7 observations,'' *Ocean-Air Interactions*, vol. 1, pp. 95-108, 1987.

Snyder, W. C., Z. Wan, Y. Zhang, and Y.-Z. Feng, ''Classification-based emissivity for land surface temperature measurement from space,'' *Int. J. Remote Sens.*, vol. 19, no. 14, pp. 2753-2774, 1998.

TABLE I. Errors in the AGEMA-measured temperature images of a blackbody at temperatures 10, 25, and 40 °C.

blackbody T (°C)	mean T	mean std δT	max std δT IN THE SEGMENT	max δT	min δT
Part A: 256 image frame segments (120 lines by 120 pixels)					
40	39.64	0.073	0.324	0.92	-0.99
25	24.71	0.091	0.333	1.49	-0.95
10	9.66	0.106	0.421	2.10	-2.86
Part B: 16 frame segments each averaged from 16 frames (120 lines by 120 pixels)					
40	39.64	0.047	0.312	0.73	-0.67
25	24.71	0.058	0.283	1.11	-0.66
10	9.66	0.060	0.343	1.90	-2.08
Part C: 256 image frame segments (averaged to 60 lines by 60 pixels)					
40	39.64	0.051	0.116	0.38	-0.37
25	24.71	0.071	0.129	0.49	-0.45
10	9.66	0.076	0.167	0.78	-0.93
Part D: 16 frame segments each averaged from 16 frames (60 lines by 60 pixels)					
40	39.64	0.041	0.111	0.31	-0.30
25	24.71	0.049	0.111	0.39	-0.31
10	9.66	0.046	0.130	0.58	-0.76
Part E: 256 image frame segments (averaged to 30 lines by 30 pixels)					
40	39.64	0.044	0.056	0.30	-0.21
25	24.71	0.062	0.084	0.33	-0.28
10	9.66	0.062	0.079	0.48	-0.36
Part F: 16 frame segments each averaged from 16 frames (30 lines by 30 pixels)					
40	39.64	0.038	0.050	0.25	-0.15
25	24.71	0.044	0.071	0.24	-0.20
10	9.66	0.038	0.062	0.31	-0.29

TABLE II. Field campaigns planned for 1999 and 2000.

time	site	purpose	airborne sensor(s)	field measurements
9/20/99 - 10/15/99	Railroad Valley, NV	LST validation	MAS, AVIRIS	LST, radiance
9/20/99 - 10/15/99	area of Mono Lake, CA	LST validation	MAS, AVIRIS	LST, radiance
February/March 2000	area of Mono Lake, CA	vicarious calibration	MAS, AVIRIS	LST, radiance
May 2000	Uyuni Salt Flats, Bolivia	vicarious calibration		LST, radiance
June/July 2000	Railroad Valley, NV	LST validation	MAS, AVIRIS	LST, radiance
April-June 2000	Mauna Loa, Hawaii	calibration/validation	MASTER	LST, radiance
August 2000	Salt Pans, Botswana	LST validation	MAS	LST, radiance

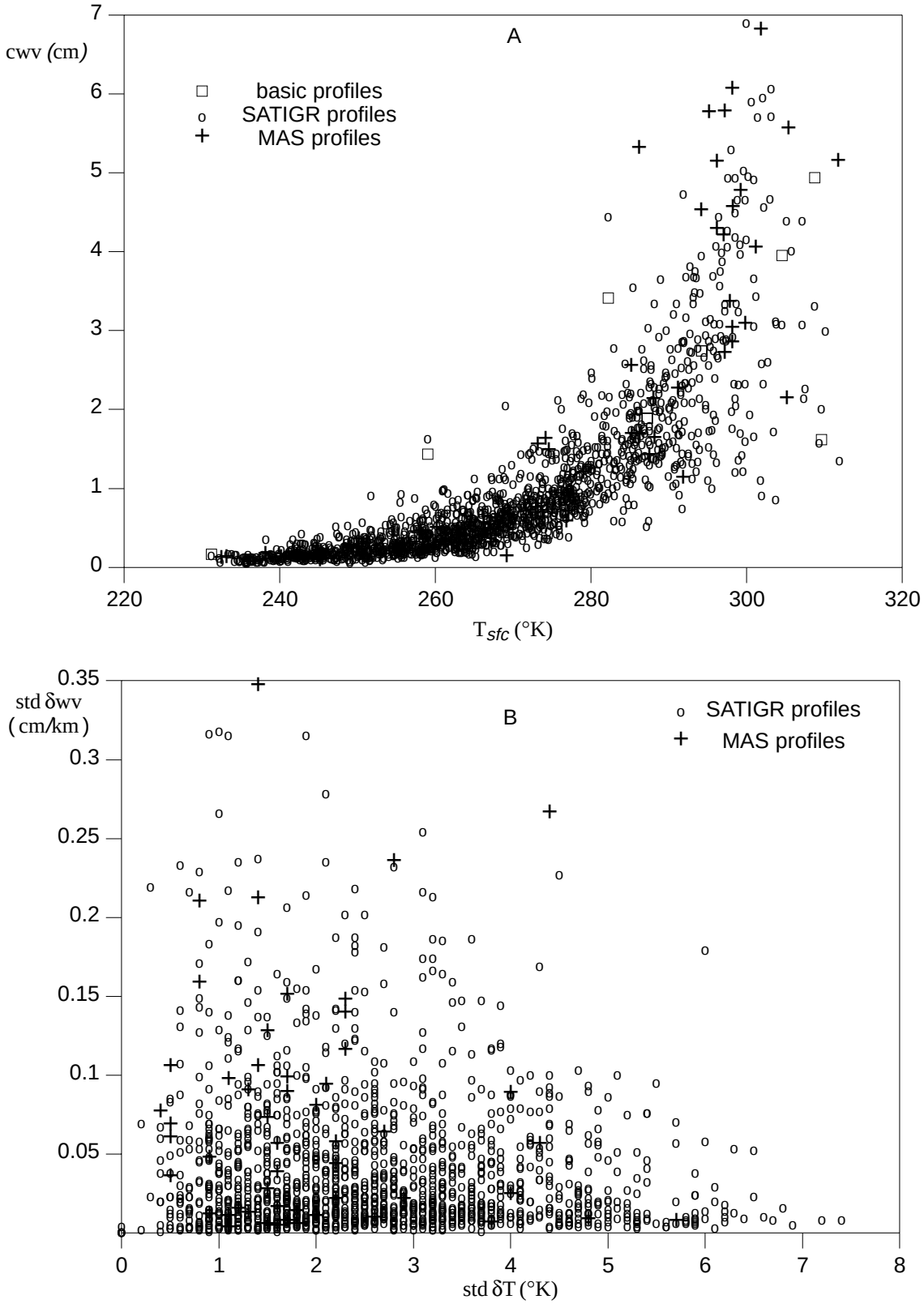

Figure 1, Air surface temperature and column water vapor (A), and the errors in temperature and water vapor profile fitting (B).

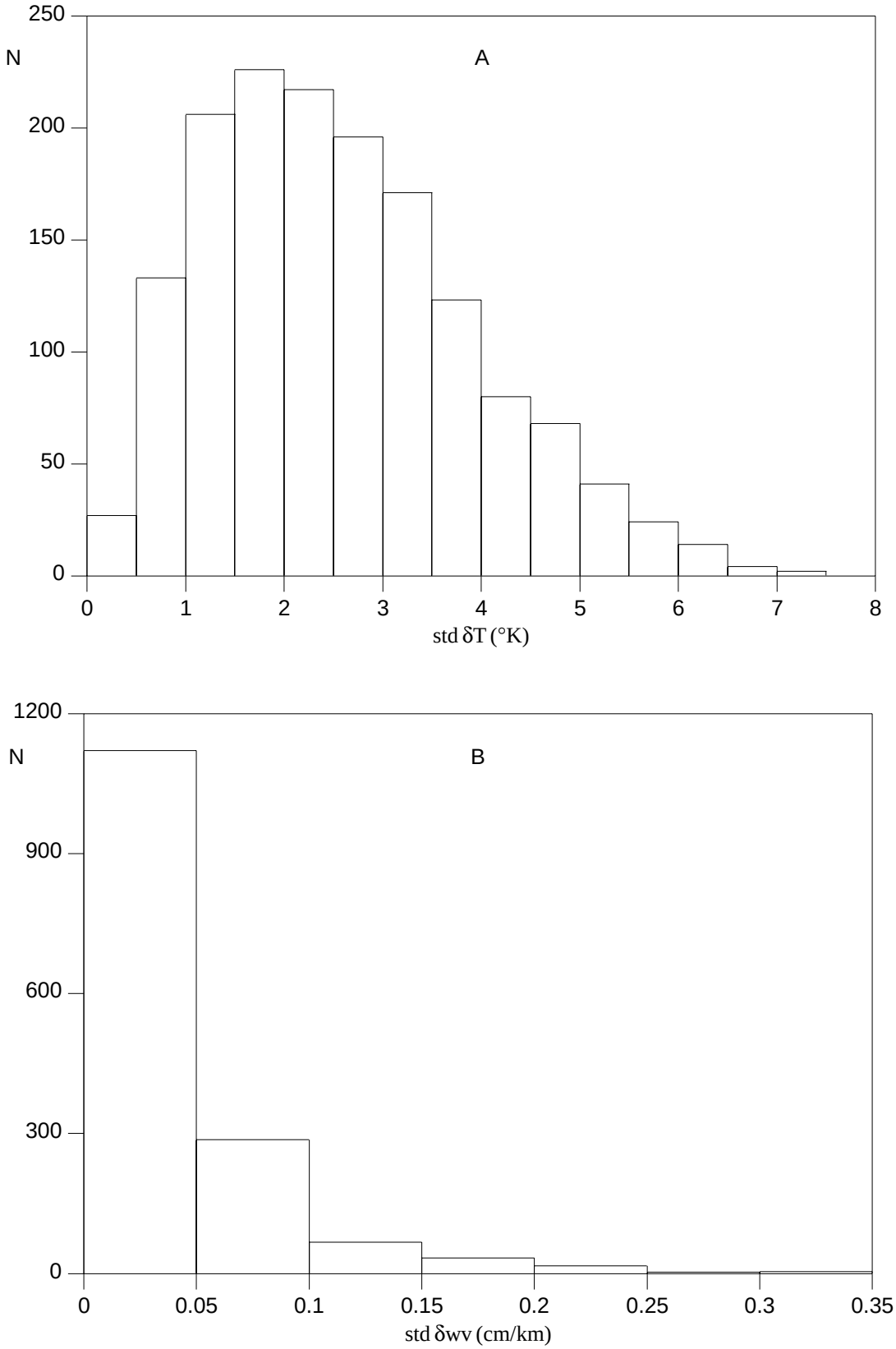

Figure 2, histograms of the errors in temperature profile (A) and water vapor profile (B) fittings.

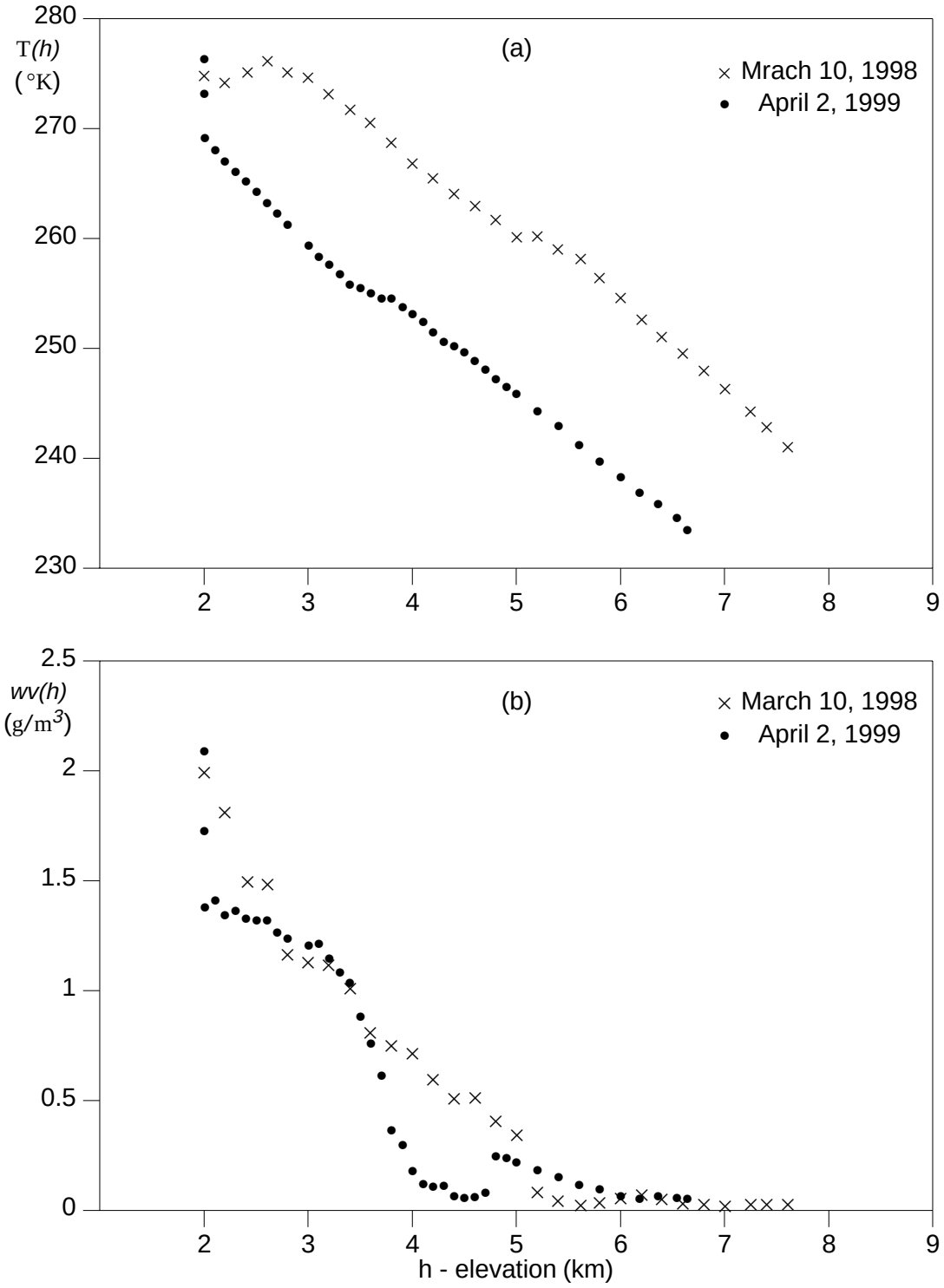

Figure 3, Atmospheric temperature (a) and water vapor (b) profiles near Mono Lake, March 10, 1998, and April 2, 1999.

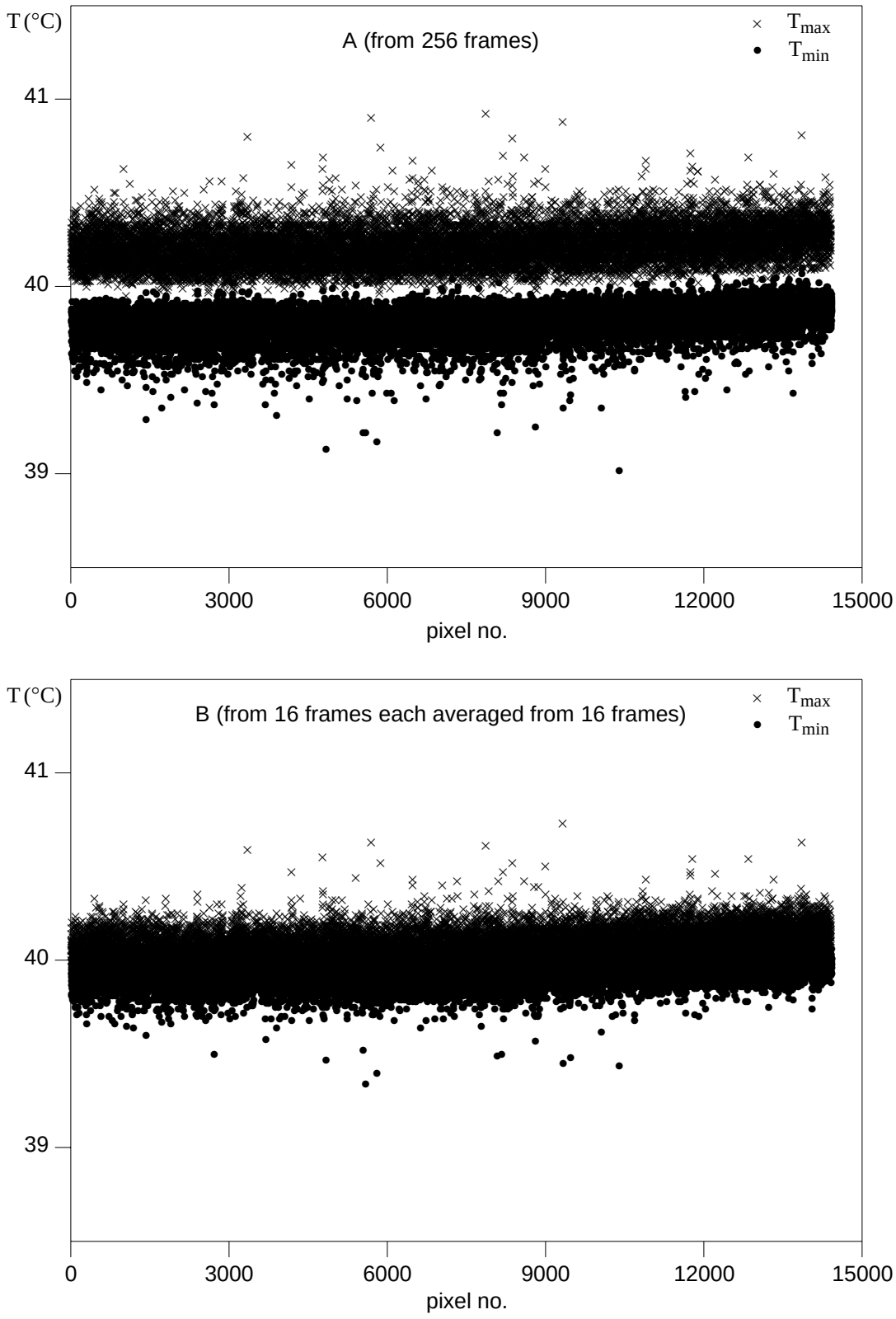

Figure 4, Maximum and mininum temperature values of blackbody at 40 °C measured by the Agema IR camera.

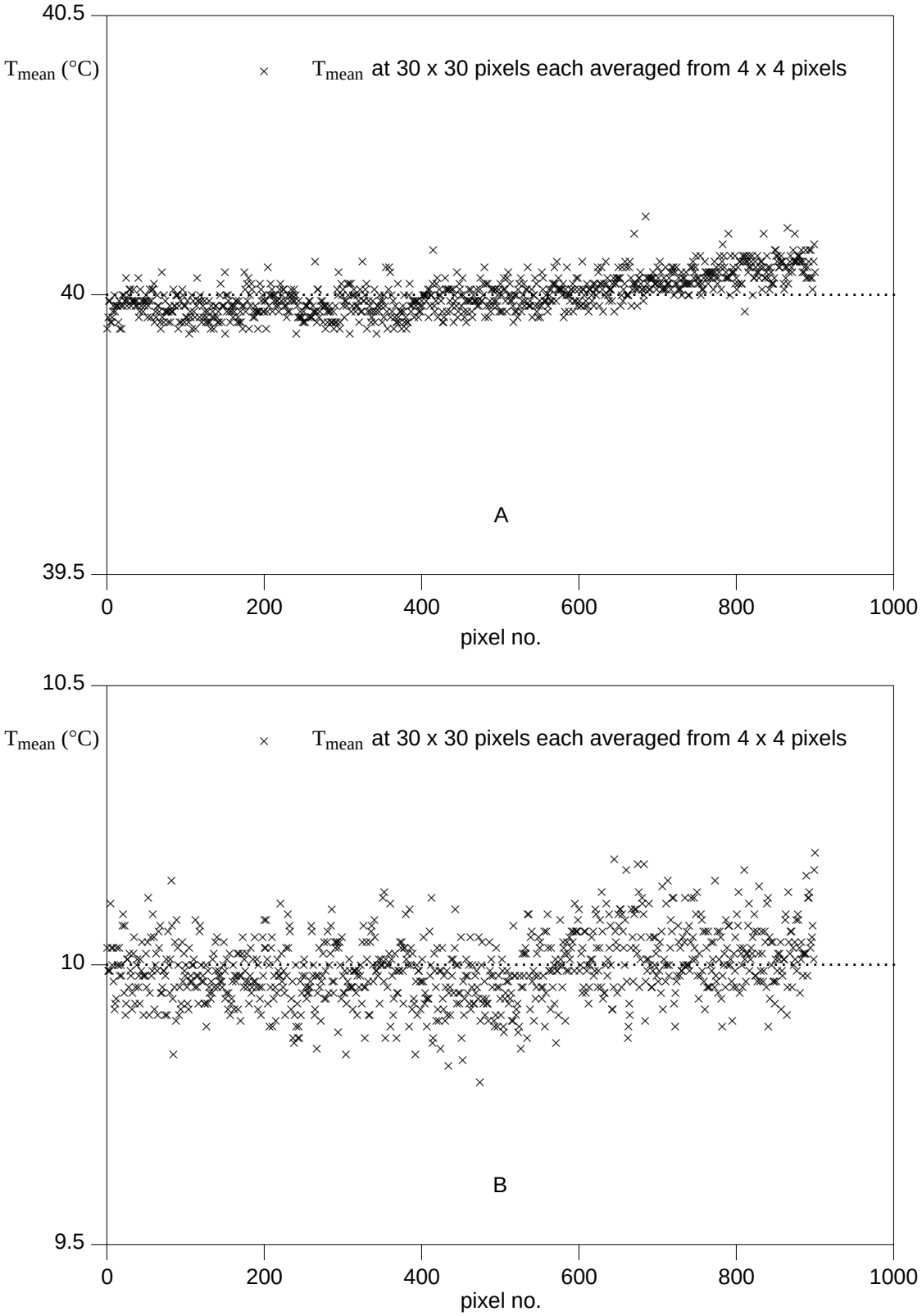

Figure 5, Temperatures of a blackbody at 10 and 40 °C averaged from 100 images measured by the AGEMA IR camera.